

Novel Styrylquinoline Derivatives as Potential Anticancer Agents, *In-Silico* studies by 3D-QSAR, Molecular Docking, and Molecular Dynamics Simulations

G. Amina^a, E.A. Abdellah^{b,*}, H. El Ghalia^a, E.H. Hicham^c, C.H. Oussama^a, B. Mohammed^d and O. Abdelkrim^a

^aEngineering Laboratory of Organometallic, Molecular Materials, and Environment, Sidi Mohamed Ben Abdellah University, Faculty of Sciences, Fez, Morocco

^bLaboratory of Processes, Materials, and Environment (LPME), Faculty of Science and Technology, Sidi Mohamed Ben Abdellah University, Fez, Morocco

^cMCNS Laboratory, Faculty of Science, University Moulay Ismail, Meknes, Morocco

^dEST Khenifra, Sultan Moulay Sliman University, Morocco

(Received 19 November 2022, Accepted 29 December 2022)

Cyclin-dependent kinase 2 (CDK2) has been recognized as a promising candidate for cancer treatment. Thus, this study sought to identify new anticancer drug candidates. For this purpose, a three-dimensional quantitative structure-activity relationship (3D-QSAR), molecular docking, and molecular dynamic (MD) simulations were employed to simulate the interaction between CDK2 and styrylquinoline to identify novel anticancer agents. The best 3D-QSAR models were performed via comparative molecular field analysis (CoMFA) and comparative molecular similarity indices analysis (CoMSIA) with elevated values of $Q^2 = 0.580$ and 0.68 and $R^2 = 0.90$ and 0.91 , sequentially. The predictive ability of the models was tested by Y-randomization and external validation employing a test set of nine molecules with a predicted determination coefficient (R_{test}^2) of 0.99 and 0.94 for CoMFA and CoMSIA, respectively. The molecular docking approach was conducted with SYBL-X.2 to enhance the analysis obtained from CoMFA and CoMSIA contour maps and perform an *in silico* search to gain insight into the nature of inhibitor interaction with enzymes. Furthermore, the performance and strength of active molecules were tested by performing MD simulations. This study offers some insight into designing new potent compounds.

Keywords: CDK2, 3D-QSAR, Molecular docking, MD simulations

INTRODUCTION

Cancer is considered the leading cause of death and a growing risk to health in the world. According to the WHO survey, approximately 18.1 million patients were diagnosed with and 9.6 million died of cancer in 2018 [1]. Despite considerable improvements in cancer therapies, cancer death rates are increasing rapidly worldwide [2]. Hence, there is an urgent need to find modern and potentially effective anticancer agents to overcome tumor resistance. Inhibition of

CDK2 is a powerful strategy to get rid of malignancy [3].

CDK2 is a member of the threonine protein kinases and serves a crucial function in modulating the evolution of cell cycle and controlling cell growth. Therefore, CDK2 inhibitors can be considered potential antitumor agents [4]. Consequently, medicines such as flavopiridol, roscovitine, olomoucine, adapalene, and kenpaullone, which are considered to be CDK2 inhibitors, have been found to trigger the downregulation of the enzyme through a variety of processes and, thus, have been used to treat malignancy [4-7]. The non-specificity and the toxic nature of the majority of these medications highlight the need for more particular and less toxic candidates [8]. The challenge to find a new potent

*Corresponding author. E-mail: abdellah.elaissouq@usmba.ac.ma

antitumor drug can be addressed by using computer-aided drug design approaches [9]. In addition, some researchers have explored the potential of heterocyclic compounds, such as styrylquinoline, as excellent candidates against cancer. As a result, styrylquinoline has attracted the interest of synthetic organic chemists due to the growing need for further biological research.

Styrylquinoline is a heterocyclic aromatic organic compound with the molecular formula of C_9H_7N [10]. Along with the listed heterocyclic structures, styrylquinoline derivatives represent a group of compounds that have received increasing attention recently [11]. Styrylquinoline derivatives have been extensively investigated in a variety of domains, especially in the medicinal field [12]. Styrylquinoline derivatives are known for having a number of response sites, which allow them to have significant interaction and turn them into exceptional antecedents in the synthesis of novel heterocyclic compounds. Due to their important biological characteristics, heterocyclic compounds have been used in the treatment of malaria [13] and cardiovascular diseases [14] and utilized as antimycotic [15], antiseptic [16], anticancer [17], and antimicrobial [18] agents. They are also used as corrosion inhibitors [19-20] as well as in fighting pathogenic bacteria and microbes [18]. Recent studies show that styrylquinoline is effective in treating malignancy, which suggests that styrylquinoline can potentially be used for drug treatment in the future. Therefore, further experimental data on the anticancer activity of styrylquinoline derivatives may be helpful in the design of novel compounds with antitumor activity. Computational chemistry tools enable us to extract the most relevant data from a large collection of experimental data and use them in designing novel candidate compounds. The quantitative structure-activity relationship (QSAR) model has been widely used in drug discovery and development. In this regard, QSAR has great applicability in correlating molecular information with biological activities and is considered as an effective tool in both understanding the mechanism of action of drugs and designing novel drugs with robust properties. Several robust QSAR models have been introduced over the past years that include a broad range of biological and physicochemical activities. Three-dimensional (3D)-QSAR remains a highly efficient and widely used computational tool in virtual screening as well

as in designing new drugs and inhibitors. Therefore, in this study, a 3D-QSAR model was performed on a series of styrylquinoline derivatives with antitumor activity against cancer cells to explore the relationship between their chemical structure and activities based on the CoMSIA and CoMFA contour maps generated in the SYBYL software. In addition, the dynamic study and steadiness of the compounds were done by MD simulations. A molecular docking model, which provides 3D pictorial data of molecular binding mode, was applied to simulate the binding mode of compounds. Molecular docking studies reveal different aspects of the ligands within the active area, which assists researchers to hypothesize the potential interactions between receptors and ligands [21-22].

MATERIALS AND METHODS

Data Sets Preparation

A database of 48 derivatives of 5,6,7-trimethoxy-N-aryl-2-styrylquinoline-4-amines (TASQA) was selected for their anticancer activity against A-2780 [23]. All activity values were transformed to the negative logarithm of IC₅₀ ($pIC_{50} = -\log_{10}(IC_{50})$) and then utilized as dependent variables in the 3D-QSAR study. The dataset was randomly divided into the training and test sets to create a 3D-QSAR model and evaluate its predictive ability. Before modeling, the structures of all compounds were plotted, using ChemSketch software, and then optimized by molecular mechanics (MM2) integrated into the ChemBiooffice software.

Minimization and Alignment

The structure of each of the 48 compounds was minimized using Tripos force field [24] with a convergence criterion of 0.01 kcal mol⁻¹ Å and a maximum number of 2000 iterations [21]. Partial atomic charges were calculated using Gasteiger-Huckel charges [25]. The chemical structures of the studied compounds are shown in Fig. 1. The activity values of the 48 studied derivatives and their appropriate structures are displayed in Table 1. The main potential compound (N° 43) was taken as a template compound. The superimposed structures of the aligned database employing molecule N° 43, as a template molecule, are shown in Fig. 2.

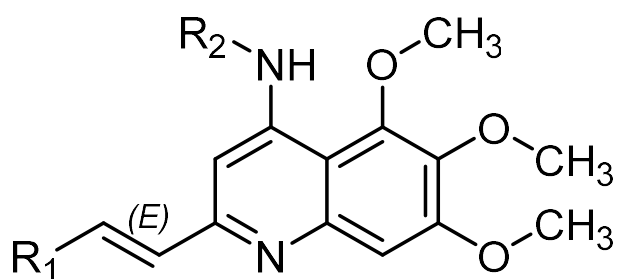


Fig. 1. The Chemical structure of the studied compound.

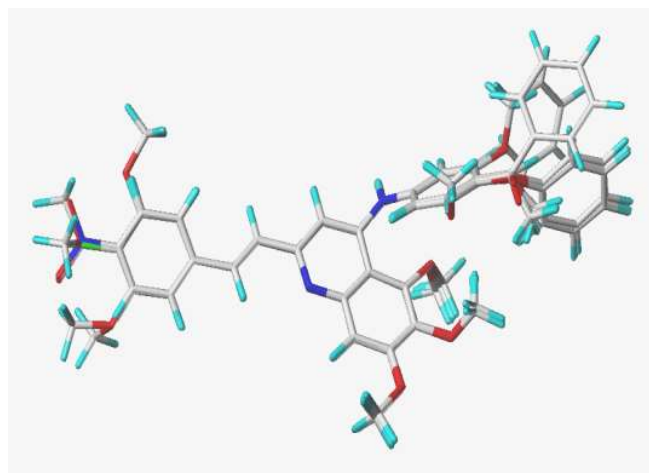


Fig. 2. Alignment following the superimposition of the 48 studied compounds employing molecule N° 43.

CoMFA and CoMSIA Studies

CoMFA is a great process for drug design. This analysis builds a 3D-QSAR model by associating the 3D steric (S) and electrostatic fields (E) with the corresponding activities. The CoMSIA is an alternative to CoMFA that exploits not only the interaction fields (S) and electrostatic fields (E) but also hydrophobic fields (H), hydrogen-bond acceptor (HBA), and hydrogen-bond donor (HBD). The CoMSIA method provides richer and easier-to-interpret results compared to the CoMFA method. The shape of the interaction fields is described in a three-dimensional mesh network with a spacing of 2 Å. The hybrid carbon Sp³ was utilized for calculating certain descriptors in CoMSIA, and the attenuation factor was set to 2.0 kcal mol⁻¹. The threshold values were set to 30 kcal mol⁻¹ [26]. The potentials depending on the space between the “probe atom” and the compound were modeled based on the Gauss method. For the steric field, Van der Waals equation was incorporated into the SYBYL-X 2.0 [27]. Several CoMFA models were created using permutations of molecules. By taking into account the variations between the compounds in the training and test sets, many CoMFA models were constructed. The criteria employed for the most excellent CoMFA model were based on the elevated values of Q² and R² and the smallest standard error of estimate (SEE) value. Every promising combination of the five fields was evaluated, and the most perfect one was selected to develop the model [28].

Table 1. Chemical Structures and Their Corresponding Antitumor Activities of Studied Compounds

Compounds	R ₁	R ₂	pIC ₅₀	Compounds	R ₁	R ₂	pIC ₅₀
1			5.12	25			5.64
2			5.25	26*			4.89
3			5.66	27			5.4

Table 1. Continued

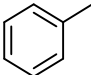
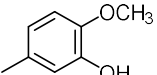
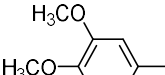
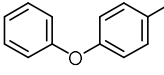
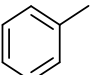
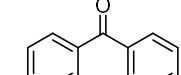
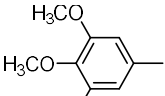
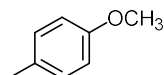
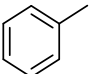
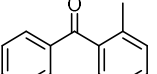
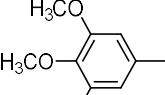
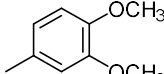
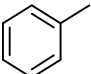
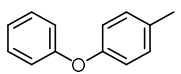
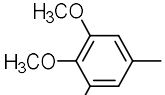
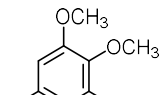
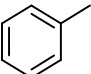
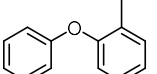
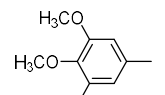
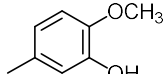
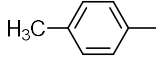
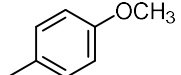
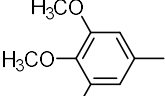
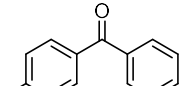
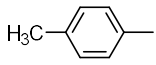
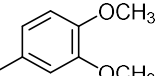
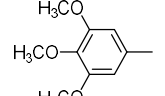
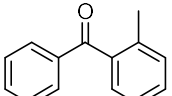
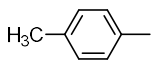
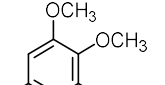
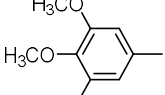
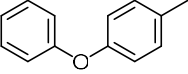
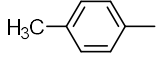
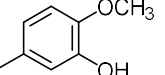
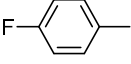
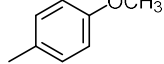
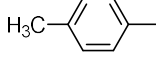
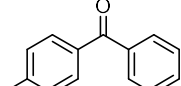
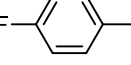
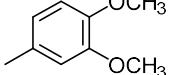
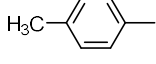
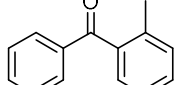
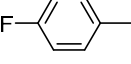
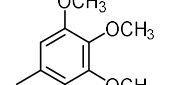
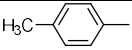
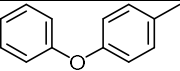
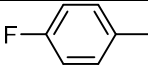
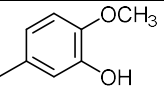
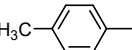
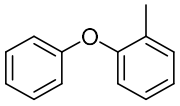
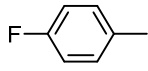
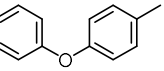
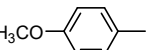
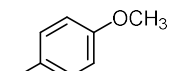
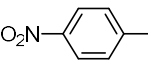
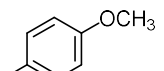
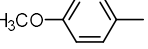
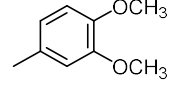
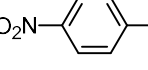
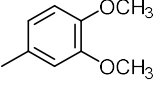
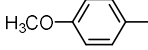
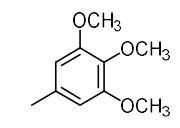
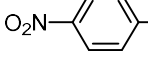
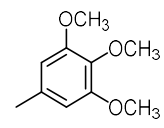
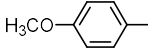
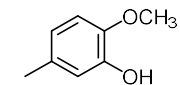
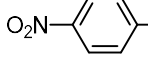
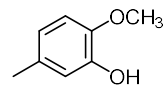
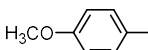
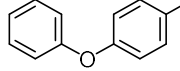
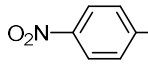
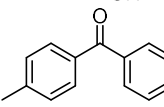
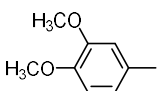
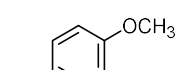
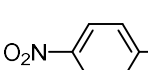
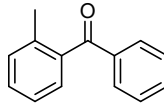
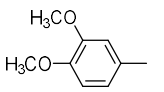
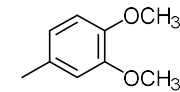
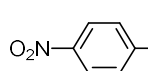
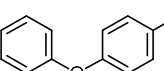
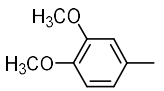
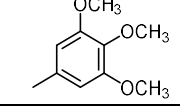
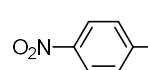
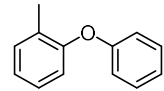
4			5.48	28			5.15
5			4.18	29			5.40
6			4.99	30			5.54
7			4.97	31*			5.83
8			5.04	32			5.71
9			5.34	33			4.85
10			5.51	34			4.6
11			5.88	35*			5.39
12			5.63	36			5.49
13			4.53	37*			5.9
14			4.96	38			5.97

Table 1. Continued

15			5.14	39*			5.93
16			4.92	40*			4.93
17			5.36	41			5.5
18			5.46	42			5.84
19			5.66	43*			6.42
20			5.46	44			5.13
21			5.06	45*			5.04
22			5.52	46			5.02
23			5.77	47*			5.42
24			6.30	48			4.73

Partial Least Square (PLS) Analysis

PLS analysis is an expansion of multiple regression analysis [29]. In this study, this statistical process was used to estimate the linear correlation between the CoMFA and CoMSIA descriptors and their cytotoxic activity. PLS analysis was performed to develop the most efficient CoMFA and CoMSIA models. The highest value of Q^2 (cross-validation correlation coefficient), the lowest SEE, and the least number of components were the three parameters taken into consideration to choose the best 3D-QSAR models. A model with elevated internal predictive capacity and a high coefficient of determination (R^2) is necessary but not enough. Several external validation criteria were used to test the

statistical robustness of the selected model.

External Validation (Prediction)

The major goal of a 3D-QSAR model is to predict the biological properties of newly designed/suggested compounds. Once a QSAR model is built, the next step is to study its predictive ability. In practice, the simplest way to examine external validation is to check the model on a subgroup of compounds (test set) that has not been applied throughout the development of the model [30-31]. The statistical metrics obtained from the analysis provided us with some insights into the predictive ability of the selected model. R_{test}^2 is the most frequent statistic used for linear

models.

Y-Randomization

Y-Randomization is an extensively employed method to assess the credibility of QSAR models [32]. In this tool, the dependent-variable vector (descriptors matrix) and the Y-vector (activity response) are randomly shuffled and a new model is created by the new independent variable matrix. The procedure is frequented numerous times. It is predicted that the consequential models will generally have a small determination coefficient and small Q^2 values. In rare cases, a high Q^2 value may be obtained due to an uncertain correlation or a structural repetition of the learning group. Assuming that all the proposed models have high R^2 and LOO Q^2 values, it is significant if an approvable model is unable to account for a given dataset.

Applicability Domain

The applicability domain (AD) of a QSAR model must be relative to the 3rd OECD principle and connected with a distinct field of applicability. Since no specific method exists to describe the AD, numerous modes of action have been suggested in the literature [33]. The most common values used to describe the AD of the proposed models are the leverage values.

Molecular Docking

Every modeling study was performed through the SYBYLX 2.0 molecular. This research was focused on the interaction between the active position of Cyclin-dependent kinase 2, as the enzyme, and the inhibitors to form a stable complex. Initially, the CDK2 was uploaded from the PDB protein databank of the RCSB with the entry code 6GUH.

The 3D-structure of the CDK2 was specified by X-ray diffraction with a resolution of 1.5 Å, and a protein monomer emerged with 284 residues and 2548 atoms. It was co-crystallized with the inhibitor 4-(2-methyl-3-propan-2-yl-imidazol-4-yl)-{N}-(4-methylsulfonylphenyl)pyrimidin-2-amine ($C_{18}H_{21}N_5O_2S$). The water molecules and cofactors were detached to find a carcass of CDK2.3D-structure of compound 43, which had the best experimental activity against cancer, using the ChemDraw, Then, it was optimized in the Tripos standard force field [24]. Therefore, the protein-ligand binding site was investigated and conceived *via* the

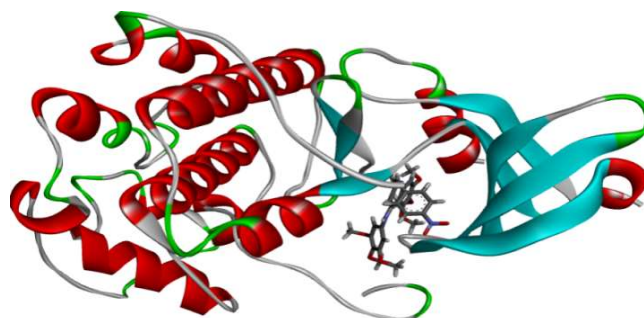


Fig. 3. The location of the template in the 6GHU receptor.

Discovery Studio software [34]. The preliminary study of the interaction between the template and the 6GHU receptor showed that the compound had penetrated well into the receptor (Fig. 3).

Molecular Dynamics Simulation

The Protein Data Bank gives the crystal structure of the receptor complex. The complex structure was subjected to MD simulation by the Amber package [35]. The system was neutralized by the addition of Na^+ counter ion, and the TIP3P water model was utilized. The ff14SB force field was applied to the protein ligands complex. The system was energy reduced by the steepest descent algorithm. A limiting simulation of the site was used to balance the system and solvent in line with the protein to the actual simulation. Particles mesh Ewald (PME) SHAKE algorithm was performed for hydrogen interaction [36]. CPPTRAJ and PYTRAJ were employed for RMSD and RMSF analysis, and Proteins plus Tools was used for the visualization [37].

RESULTS AND DISCUSSION

CoMFA Model

The CoMFA model was proposed to explain the correlation between the S and E fields with anticancer activity. Table 2 shows the numerical results of CoMFA as well as the most excellent CoMFA model outcome. The CoMFA model showed the highest cross-validated determination coefficient ($Q^2 = 0.58$) with 3 most select components, along with a non-cross-validated PLS analysis coefficient ($R^2 = 0.90$), F-value of 103.44, and low SEE (0.14). A set of 9 compounds resulted in a R_{test}^2 value of 0.99, suggesting that the proposed model had a good

Table 2. Arithmetic Criteria of CoMFA and CoMSIA Models Employing the PLS Technique

Model	Q^2	R^2	SEE	F	ONC	R_{test}^2
CoMFA model	0.58	0.90	0.14	103.4	3	0.99
CoMSIA model	0.68	0.91	0.13	54.42	6	0.94

predictive ability. The plot of the correlation between the expected and observed activity of the CoMFA model is shown in Fig. 4.

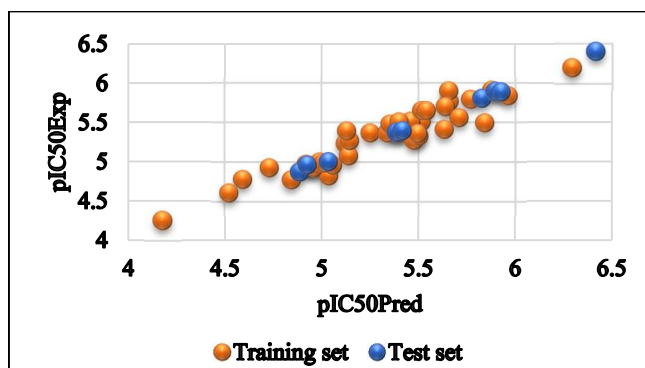
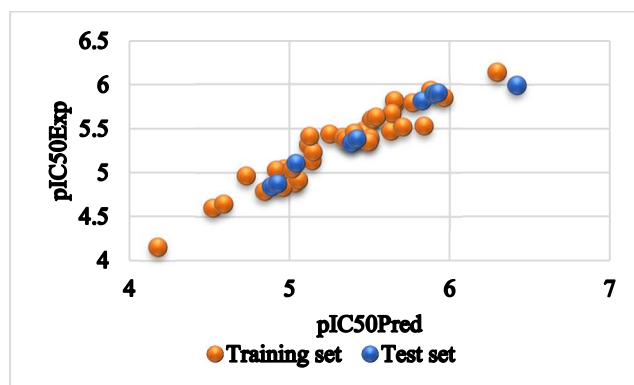
CoMSIA Model

CoMSIA analysis was considered as an extension of CoMFA and was generated and proposed to clarify the S, E, H, HBA, and HBD effects of the substituent on the anticancer activity of 48 compounds.

The results of the CoMSIA model are summed up in Table 2. Based on the results, when the non-cross-validated R^2 was 0.91, the standard error was 0.13, and the Fisher ratio was 54.42, the CoMSIA model exhibited a high cross-validated Q^2 of 0.68, with six optimal components. Meanwhile, the predictive ability of the developed model was established by employing external validation, with an R_{test}^2 value of 0.94, which indicates the perfect sturdiness and the powerful predictive ability of the developed model. The association of the predicted and observed activity of the CoMSIA model is shown in Fig. 5.

The Graphical Interpretation of CoMFA and CoMSIA

To obtain information about the favorable and unfavorable zones for anticancer activity, CoMFA and CoMSIA contour maps were created. Modifications in the structure of molecules led to some changes in the physicochemical proprieties of compounds, which, in turn, increased or decreased the cytotoxic activity. The E and S contour maps of CoMFA, and the S, the E, and the HBA contour maps of CoMSIA are illustrated in Figs. 6, 7, and 8, respectively. Compound 43, as the main active compound, emerged as a template for the whole set of compounds; thus, it was used as the reference structure.

**Fig. 4.** Observed and predicted pIC50 values.**Fig. 5.** The observed and predicted pIC50 values.

Steric Contour Maps

The steric interactions are represented by green and yellow colors. Green contours (80% contribution) show positions where immense groups increased the activity while yellow contours (20% contribution) show positions where the bulky groups reduced activity. The steric contour maps of CoMFA and CoMSIA models are presented in Figs. 6a and 6b, respectively.

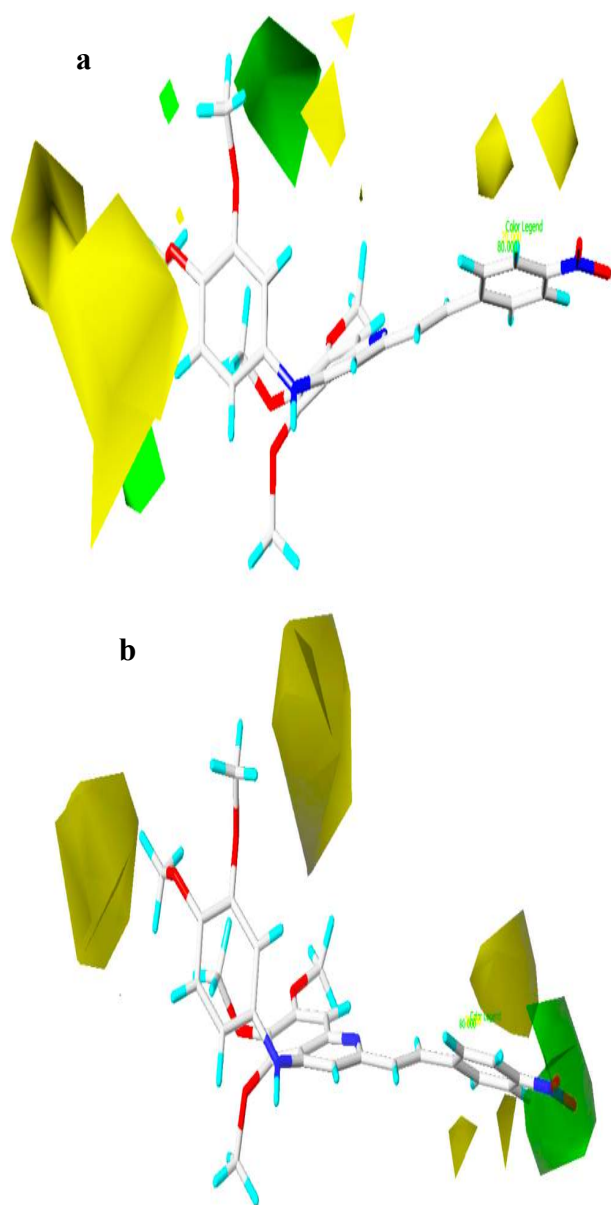


Fig. 6. Steric contour maps of CoMFA (a) and CoMSIA (b) of compound 43.

The green region around the oxygen of the nitrogen dioxide indicates that the bulky substituent could increase the anticancer activity while two yellow contours pears close to the methoxy methane were found to be sterically unfavorable for increasing PIC_{50} values. Based on the above findings, the compound with methoxymethane at R_1 substituent (*e.g.*, compounds 11, 24, 31, and 32) revealed the best activity

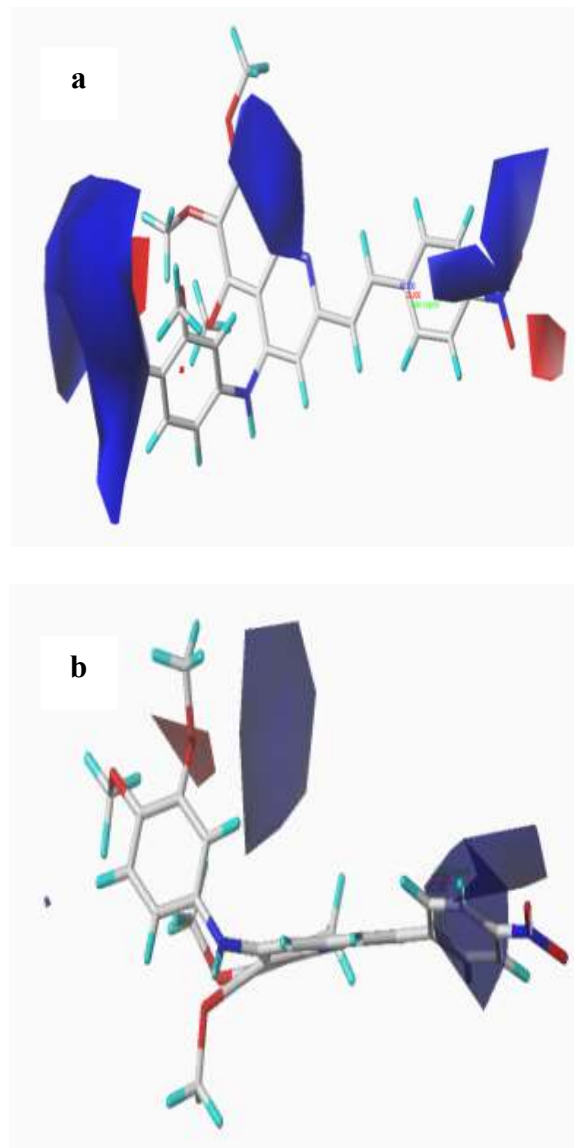


Fig. 7. Electrostatic contour maps of CoMFA (a) and CoMSIA (b) around compound 43.

compared to the compounds with toluene at R_1 substituent (*e.g.*, compounds 5, 6, and 7).

Electrostatic Contour Maps

The electrostatic interactions of CoMFA and CoMSIA are demonstrated in Figs. 7a and 7b, respectively. The red color contour shows the favorable sites for the electronegative groups whereas the blue color contour shows the site where adding electropositive groups decreased the anticancer activity.

The red form covers the oxygen present in the methoxymethane, signifying that the electronegative groups in this site could improve the anticancer activity. However, the presence of the blue contour around the 1-methyl-3-nitrobenzene highlights the site where the creation of more negative electrostatic decreased the anticancer activity. The dataset explains why compounds 24, 39, 31, and 23 were more active than compounds 5, 6, 7, and 26.

H-Bond Acceptor Contour Maps

The HBA contour maps of the CoMSIA model are displayed in Fig. 8. The large purple contours around the nitromethane and 1-methyl-3-nitrobenzene increased the anticancer activity while the red contour close to ethane represents the HBD group.

Y-Randomization

The randomization analysis was performed to ensure that the relationship between the descriptors and the anticancer activity presented by the developed model was not due to chance. The principle of this test was based on randomly mixing the observations of the learning series 100 times, and the results are presented in Table 3. The model chosen in this study was robust since the obtained R^2 and Q^2 values were less than those of the validation thresholds, suggesting that the predictive ability of the developed QSAR model was not the result of accidental correlations.

The AD was assessed by a leverage study revealed as a Williams plot, in which standardized residuals and leverage threshold values $h^* = 0.25$ were drawn from Fig. 9. It is worth noting that there were four compound outliers, all in the training set. Compounds N° 24, 48, and 5 had a standard deviation outside ± 2 .

Docking Studies

This study was utilized the molecular docking technique for the forecast of promising interaction modes between styrylquinolines derivatives stand on pyrimidine and the active position of the enzyme, and that explains why the SYBYL X.2 software was used in this study.

It seemed it was a good idea to dock compound 43 which has the most excellent activity (IC₅₀) against cancer cell lines (A2780). The visual examination Fig. 10 illustrates that the molecule 43 makes four H-bond with the active spot of the

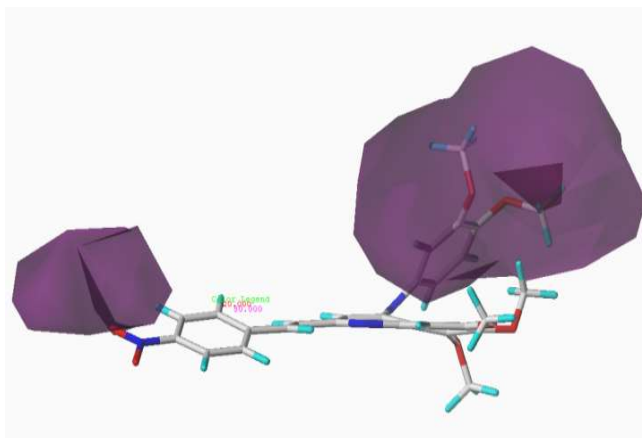


Fig. 8. HBA contour maps of the CoMSIA model around compound 43.

Table 3. The Results of Y-Randomization Analysis for the CoMSIA Model

Average	R	R ²	Q ²	cR _p ²
	0,424	0,235	-0,111	0,819

enzyme, the initial one is produced between the oxygen of the substituent NO_2 of the inhibitor and the carbonyl group of the residue GLU A:8, separated by a space of 2.7 Å. The next one was recognized between the carbonyl group of the residue GLU A: 12 and the Methyl group of the inhibitor, alienated by a distance of 2.5 Å. The third interaction was found to be between the amide function of the residue GLN A: 131 and the Methyl group of the inhibitor, alienated by a distance of 2.46 Å. The fourth H-bond interaction was created between carboxyl groups of the residue ASP A: 145 and the Methyl group of the inhibitor, estranged by a distance of 2.5 Å.

It is also important to highlight the role of the residues HIS A: 84, LEU A: 134, ILE A: 10, VAL A: 18, and GLN A85 in the stability of the CDK2-compound 43 complex by participating in the configuration of several interactions of type Pi-alkyle, pi-sigma, amide pi-stacked and van der Waals.

The pink color in Fig. 11 shows the positions where HBD groups are enviable; otherwise, the brown color shows the position where H groups are preferable.

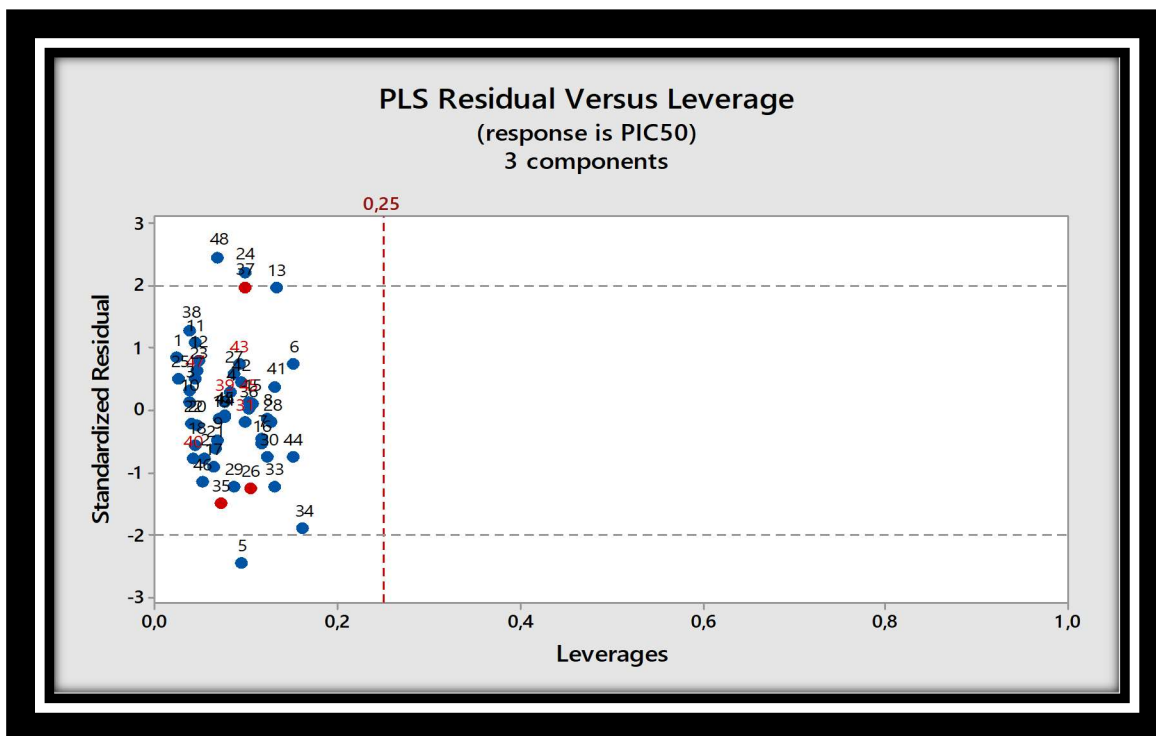


Fig. 9. The Applicability Domain of COMSIA model/SEA.

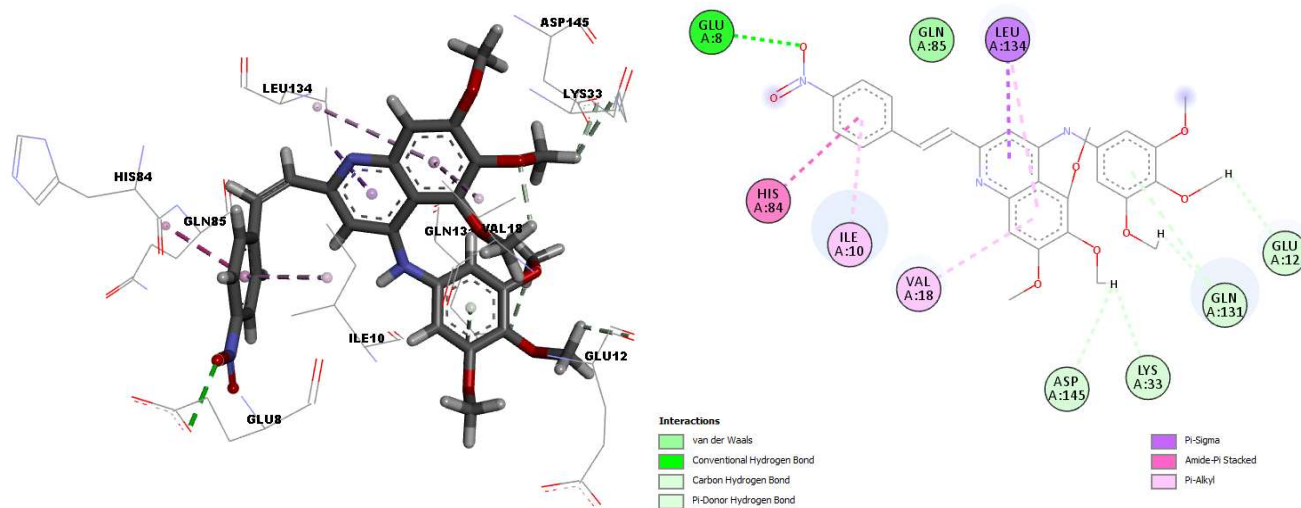


Fig. 10. A variety of interactions created between compound 43 and the active position of CDK2.

MD Simulation

To recognize the binding mode of CDK2 with 6GUH, a docking simulation was performed which directed this ligand into the active site of the protein. The docking analysis predicted that CDK2 formed 2 H-bond interactions with the

Lys44, Thr22, and Tyr183 residues sited in the binding pocket. In the docking, the impact of solvent on the ligand and protein was not completely taken into consideration; therefore, the MD simulation was established to check the steadiness of the molecule in the aqueous solution. MD

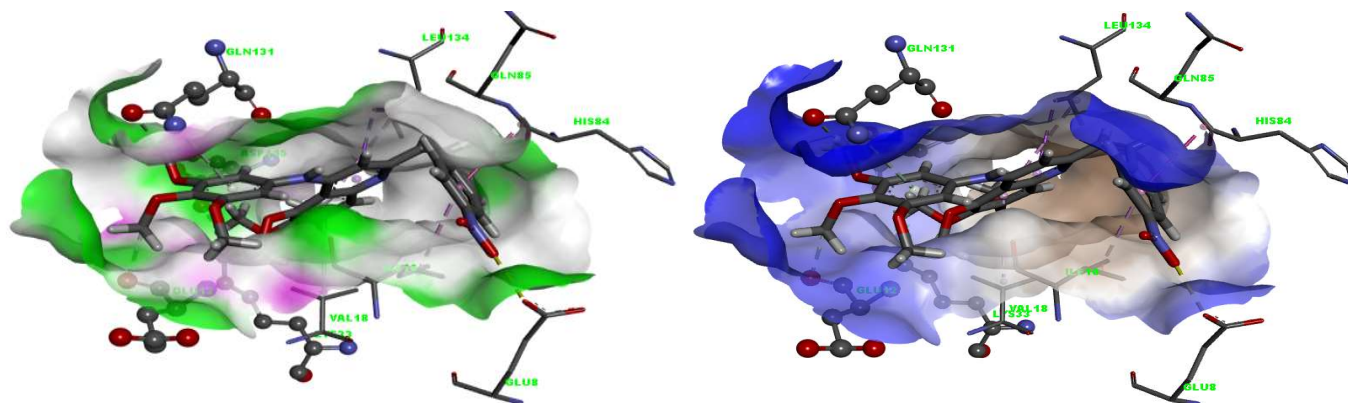


Fig. 11. The hydrophobic and H-binding surfaces of the template and the 6GUH-CDK2.

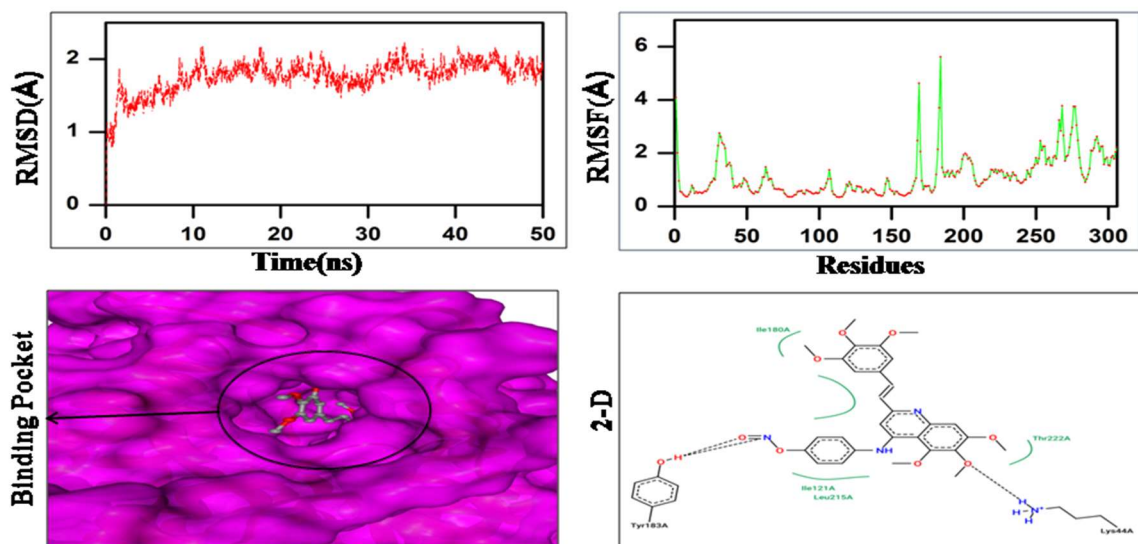


Fig. 12. RMSD and RMSF for the receptor complex. The average RMSD and RMSF values rose to 2 Å, and 5 Å respectively. The binding pockets after the simulation are also shown in the figure.

simulation procedure was invested to find a dynamical image of the conformational modification that happen in 6GUH-CDK2 complex in aqueous solution, with the aim of discovering the conformational modification that happened in the receptor and CDK2. The RMSD of the trajectory with the esteem of their original structure varied from 0.8 to 2 Å.

After 10 ns MD simulation, the RMSD value rose to 2 Å; however, further fluctuation was not observed until the end of MDS, suggesting that the compound reached its stability after 30 ns. After the completion of 50 ns simulation, the most stable and energy-minimized conformer was achieved, and

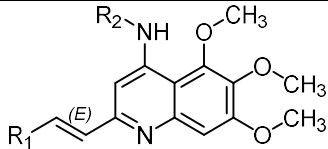
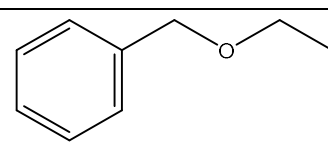
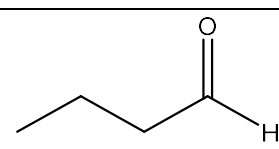
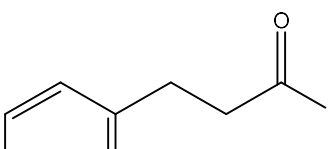
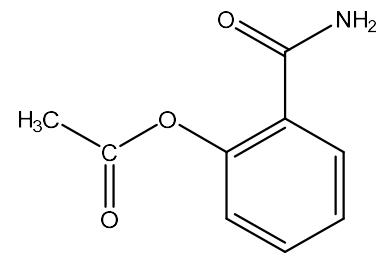
post-simulation analysis was carried out to investigate the receptor complex interface and suggest any prominent change that could have occurred during the simulation.

The residual flexibility was obtained by RMSF. The average RMSF for the receptor complex was viewed to be 1 and 5 Å. The Lys44, Thr22, and Tyr183 residues lowered flexibility was due to deferential dynamics upon the binding of ligand (Fig. 12).

Development of New Inhibitors

The results of the CoMFA and CoMSIA models and

Table 4. Designing of New Potent Compounds

			
Compounds	R1	R2	pIC_{50}
X1			6.75
X2			6.83

docking molecular studies can be used to obtain information concerning the structural features controlling the anticancer activity. In addition, the results of such studies can be used to recommend new candidate drugs with potent anticancer activity. According to the dataset obtained from the 3D-QSAR models, a new candidate drug was designed with high anticancer activity. The newly developed potent compounds and their anticancer activity are listed in Table 4.

CONCLUSION

In this study, 3D-QSAR, molecular docking, and MD simulations were performed on a set of 48 derivatives of 5,6,7-trimethoxy-N-aryl-2-styrylquinoline-4-amines as antitumor agents. The CoMFA was used to calculate the important statistical quality of both S and E fields with the anticancer activity and perfect predictive ability ($Q^2 = 0.58$, $R^2 = 0.90$). The COMSIA model with the best predictive ability exhibited statistically significant reliability of S, E, and HBA ($Q^2 = 0.68$, $R^2 = 0.91$). Based on the results of the 3D-QSAR models, a number of new derivatives were designed with improved anticancer activity. The results of this research may pave the way for designing new chemical candidates that can be utilized to treat tumors.

ACKNOWLEDGEMENT

The authors would like to thank the Moroccan Association of Theoretical Chemistry (MATC) for its help regarding the relevant software.

REFERENCES

- [1] Bray, F.; Ferlay, J.; Soerjomataram, I.; Siegel, R. L.; Torre, L. A.; Jemal, A., Global Cancer Statistics: Globocan Estimates of Incidence and Mortality Worldwide for 36 Cancers in 185 Countries. *A Cancer J. Clin.* **2018**, *68*, 394-424, DOI: 10.3322/caac.21492.
- [2] Corsello, S. M.; Nagari, R. T.; Spangler, R. D. *et al.*, Discovering the Anticancer Potential of non-oncology Drugs by Systematic Viability Profiling. *Nat Cancer* **2020**, *45*, 235-248, DOI: 10.1038/s43018-019-0018-6.
- [3] Meng, X.; Zhu, X.; Ji, J.; Zhong, H.; Li, X.; Zhao, H.; Xie, G.; Wang, K.; Shu, H.; Wang, X., Erdafitinib Inhibits Tumorigenesis of Human Lung Adenocarcinoma A549 by Inducing S-Phase Cell-Cycle Arrest as a CDK2 Inhibitor. *Molecules* **2022**, *27*, 6733, DOI: 10.3390/molecules27196733.

- [4] Almealmadi, S. J.; Alsaedi, A. M.; Harras, M. F.; *et al.*, Synthesis of a New Series of Pyrazolo[1,5-a]Pyrimidines as CDK2 Inhibitors and Anti-Leukemia. *Bioorg. Chem.* **2021**, *15*, 117-105431, DOI: 10.1016/j.bioorg.2021.105431 .
- [5] Eman, R.; Elmasry, F., Development of Newly Synthesised Quinazolinone-based CDK2 Inhibitors with Potent Efficacy against Melanoma. *J. Enzyme Inhib. Med. Chem.* **2022**, *27*, 686-700, DOI: 10.1080/14756366.2022.2036985.
- [6] Wagdy, M.; Eldehna, M.; Maklad, H. A; Eslam, B.; Abourehab, A. S.; El Kerday, M., Identification of 3-(piperazinylmethyl)benzofuran derivatives as novel type II CDK2 inhibitors: design, synthesis, biological evaluation, and in silico insights, *J. Enzyme. Inhib. Med. Chem.* **2022**, *12*, 1227-1240, DOI: 10.1080/14756366.2022.2062337.
- [7] Schaefer, I. M.; Hemming, M. L.; Lundberg, M. Z. *et al.*, Concurrent Inhibition of CDK2 Adds to the Anti-Tumour Activity of CDK4/6 Inhibition in GIST. *Br J. Cancer.* **2022**, *22*, 990-035, DOI: 10.1038/s41416-022-01990-5.
- [8] Tadesse, S.; Caldon, E. C.; Tilley, W.; Wang, S. Cyclin-Dependent Kinase 2 Inhibitors in Cancer Therapy: An Update. *J. Med. Chem.* **2018**, *62*, 4233-4251, DOI: 10.1021/acs. J medchem.8b01469.
- [9] Prieto-Martínez, F. D.; López-López, E.; Eurídice Juárez-Mercado, K.; Medina-Franco, J. L., Computational Drug Design Methods Current and Future Perspectives. *In silico Drug Design* **2019**, *50*, 19-44, DOI: 10.1016/j.drudis.2009.03.013.
- [10] Jain, S.; Chandra, V.; Jain, P. K.; Pathak, K.; Pathak, D., Vaidya a Comprehensive Review on Current Developments of Quinoline-based Anticancer Agents. *Arab. J. Chem.* **2019**, *12*, 4920-4946, DOI: 10.1016/j.arabjc.2016.10.009.
- [11] Sultana, F.; Reddy Bonam, S.; Reddy, V.G.; Nayak, V.L.; Akunuri, R.; Rani Routhu, S.; Alarifi, A.; Halmuthur, M.S.K.; Kamal, A., Synthesis of Benzo[d]Imidazo[2,1-b]Thiazole-Chalcone Conjugates as Microtubule Targeting and Apoptosis Inducing Agents. *Bioorg. Chem.* **2018**, *71*, 1-12, DOI: 10.1016/j.bioorg.2017.10.019.
- [12] Diaconu, D.; Antoci, V.; Mangalagiu, V. *et al.*, Quinoline-Imidazole/Benzimidazole Derivatives as Dual/Multi-Targeting Hybrids Inhibitors with Anticancer and Antimicrobial Activity. *Sci. Rep.* **2022**, *12*, 16988, DOI: 10.1038/s41598-022-21435-6.
- [13] Ceramella, J.; Mariconda, A.; Iacopetta, D.; Saturnino, C.; Barbarossa, A.; Caruso, A., Complexes Targeting Human Topoisomerases. *Bioorg. Med. Chem Lett.* **2020**, *30*, 126905, DOI: 10.1016/j.bmcl.2019.126905.
- [14] El Sayed, IE-T.; Ullah, S.; Al-Hartomy, O. A.; Hasanein, A. M.; Kahilo, K. A.; El-Naggar, M. E., Synthesis, Nanoformulations, and *In Vitro* Anticancer Activity of N-Substituted Side Chain Neocryptolepine Scaffolds. *Molecules.* **2022**, *27* (3), 1024, DOI: 10.3390/molecules 27031024.
- [15] Ajani, O. O.; Iyaye, K. T.; Aderohunmu, D. V.; Olanrewaju, I. O.; Germann, M. W.; Olorunshola, S. J.; Bello, B. L., Microwave-Assisted Synthesis and Antibacterial Propensity of N'-(s-benzylidene and s-1H-pyrrol-2-yl)Methylene)-2 PropylQuinoline-4-Carbohydrazide Motifs. *Arab. J. Chem.* **2020**, *13*, 1809-1820, DOI: 10.1016/j.arabjc.2018.01.015.
- [16] Dorababu, A., Recent Update on Antibacterial and Antifungal Activity of Quinoline Scaffolds. *Arch. Pharm.*, **2021**, *354*, e2000232, DOI: 10.1002/ ardp.202000232.
- [17] Kumar, A.; Kumar, P.; Shetty, C. R.; James, J. P.; Shetty, H. C., Synthesis, Antidiabetic Evaluation and Bioisosteric Modification of Quinoline Incorporated 2-Pyrazoline Derivatives, *Indian J. Pharm. Educ. Res.* **2021**, *55*, 574-580, DOI: 10.5530/ijper.55.2.96.
- [18] Zaman, K.; Rahim, F.; Taha, M.; Sajid, M.; Hayat, S.; Nawaz, M.; Salahuddin, M.; Iqbal, N.; Khan, N. U.; Shah, S. A. A.; Farooq, R. K.; Bahadar, A.; Wadood, A.; Khan, K. M.; Synthesis, *in Vitro* Antiurease, *in Vivo* Anti-nematodal Activity of Quinoline Analogs and their in-silico Study. *Bioorg. Chem.* **2021**, *115*, 105199, DOI: 10.1016/j.bioorg.2021.105199.
- [19] Roy, D.; Anas, M.; Manhas, A.; Saha, S.; Kumar, N.; Panda, G., Synthesis, Biological Evaluation, Structure-Activity Relationship Studies of Quinoline-Imidazole Derivatives as Potent Antimalarial Agents. *Bioorg. Chem.* **2022**, *121*, 105671, DOI: 10.1016/j.bioorg.2022.105671.
- [20] Yang, L.; Shi, P.; Zhao, G.; Xu, J.; Peng, W.; Zhang, J.;

- Zhang, G.; Wang, X.; Dong, Z.; Chen, F.; Cui, H., Targeting Cancer Stem Cell Pathways for Cancer Therapy, Signal Transduct. *Target Ther.* **2020**, *5*, 35, DOI: 10.1038/s41392-020-0110-5.
- [21] Chedadi, O.; El Aissouq, A.; El Ouardi, Y.; Bouachrine, M.; Ouammou, A., 3D-QSAR and Molecular Docking Studies of 4-Methyl Quinazoline Derivatives as PI3K α Inhibitors. *J. Indian Chem. Soc.* **2021**, *98*, 100183, DOI: 10.1016/j.jics.2021.100183.
- [22] Osman, E. A.; Abdalla, M. A.; Abdelraheem, M. O.; Ali, M. F.; Osman, S. A.; Tanir, Y. M.; Abdelrahman, M.; Ibraheem, W.; Alzain, A. A., Design of novel coumarins as potent Mcl-1 inhibitors for cancer treatment guided by 3D-QSAR, molecular docking and molecular dynamics. *Infor. Med. Unlocked* **2021**, *26*, 100765, DOI: 10.1016/j.imu.2021.100765.
- [23] Mirzaei, S.; Eisvand, F.; Hadizadeh, F.; Mosaffa, F.; Ghasemi A.; Ghodsi, R., Design, Synthesis, and Biological Evaluation of Novel 5,6,7-Trimethoxy Quinolines as Potential Anticancer Agents and Tubulin Polymerization Inhibitors. *Bioorg. Chem.* **2020**, *98*, 103711, DOI: 10.22038/ijbms.2020.43303.10168.
- [24] Stitou, M.; Toufik, H.; Bouachrine, M.; Lamchouri, F., Quantitative Structure-Activity Relationships Analysis, Homology Modeling, Docking and Molecular Dynamics Studies of Triterpenoid Saponins as Kirsten Rat Sarcoma Inhibitors. *J. Biomol. Struct. Dyn.* **2020**, *1102*, 152-170, DOI: 10.1080/07391102.2019.1707122.
- [25] Begum, S.; Jaswanthi, P.; Venkata Lakshmi, B.; Bharathi, K., QSAR Studies on Indole-Azole Analogues using DTC Tools; Imidazole Ring is more Favorable for Aromatase Inhibition. *J. Indian Chem. Soc.* **2021**, *98*, 100016, DOI: 10.1016/j.jics.2021.100016.
- [26] Muhammed, M. T.; Aki-Yalcin, E., Homology Modeling in Drug Discovery: Overview, Current Applications, and Future Perspectives. *Chem. Bio. Drug Des.* **2019**, *93*, 12-20, DOI: 10.1111/cbdd.13388.
- [27] Goudzal, A.; ElAissouq, A.; El Hamdani, H.; Hadaji, E.; Ouammou, A.; Bouachrine, M., 3D-QSAR Modeling and Molecular Docking Studies on a Series of 2,4,5-Trisubstituted Imidazole Derivatives as CK2 Inhibitors, *J. Biomol. Struct. Dyn.* **2022**, *23*, 145-237, DOI: 10.1080/07391102.2021.2014360.
- [28] El Aissouq, A.; Toufk, H.; Stitou, M.; Ouammou, A.; Lamchouri, F., *In silico* Design of Novel Tetrasubstituted Pyridinylimidazoles Derivatives as C-Jun N-Terminal Kinase-3 Inhibitors, using 2D/3DQSAR Studies, Molecular Docking and ADMET Prediction. *Int. J. Pept. Res. Ther.* **2020**, *26*, 1335-1351, DOI: 10.1007/s10989-019-09939-8.
- [29] Zhang, X.; Yan, J.; Wang, H.; Wang, Y.; Wang, J.; Zhao, Z., Molecular Docking, 3D-QSAR, and Molecular Dynamics Simulations of Thieno[3,2-b]Pyrrole Derivatives against Anticancer Targets of KDM1A/LSD1. *J. Biomol. Struct. Dyn.* **2020**, *6*, 1538-0254, DOI: 10.1080/07391102.2020.1726819
- [30] Goudzal, A.; El Aissouq, A.; El Hamdani, H. ; Ouammou, A., QSAR Modeling, Molecular Docking Studies and ADMET Prediction on a series of Phenylaminopyrimidine-(thio) Urea derivatives as CK2 Inhibitors. *Mater. Today: Proc, Xxxx.* **2022**, *51*, 1851-1862, DOI: 1016/j.matpr.2020.08.044.
- [31] El Aissouq, A.; Chedadi, O.; Kasmi, R.; Elmchichi, L.; En-nahli, F.; Goudzal, A. ; Bouachrine, M. ; Ouammou, A.; Khalil, F., Molecular Modeling Studies of C-Glycosylfavone derivatives as GSK-3b Inhibitors based on QSAR and Docking Analysis. *J. Sol. Chem.* **2021**, *50*, 808-822, DOI: 10.1007/s10953-021-01083-6.
- [32] Zaki, H.; Belhassan, A.; Benlyas, M.; Lakhli, T.; Bouachrine; M., New Dehydroabiatic Acid (DHA) derivatives with Anticancer Activity against HepG2 Cancer Cell Lines as a Potential Drug targeting EGFR Kinase Domain. CoMFA Study and Virtual Ligand-Based Screening, *J. Biomol Struct and Dyn.* **2020**, *43*, 1538-0254, DOI: 10.1080/07391102.2020.1759452.
- [33] Song, H. M.; Zhao, L. X.; Zhang, S. Q.; Ye, T.; Fu, Y.; Ye, F., Design, synthesis, structure-activity relationship, molecular docking, and herbicidal evaluation of 2-cinnamoyl-3-hydroxycyclohex-2-en-1-one derivatives as novel 4-hydroxyphenylpyruvate dioxygenase inhibitors, *J. Agric. Food Chem.* **2021**, *56*, 12621-12633, DOI: 10.1021/acs.jafc.1c04621
- [34] Elekofehinti, O. O.; Iwaloye, O.; Josiah, S. S. *et al.* Molecular Docking Studies, Molecular Dynamics and ADME/tox reveal Therapeutic Potentials of STOCK1N-69160 Against Papain-like Protease of SARS-CoV-2. *Mol Divers.* **2021**, *25*, 1761-1773, DOI: 10.1007/s11030-020-10151-w.

- [35] Vivek-Ananth, R. P.; Krishnaswamy, S.; Samal, A., Potential Phytochemical Inhibitors of SARS-CoV-2 Helicase Nsp13: A Molecular Docking and Dynamic Simulation Study. *Mol. Divers.* **2022**, *26*, 429-442, DOI: 10.1007/s11030-021-10251.
- [36] Wang, Y. L.; Wang, F.; Shi, X. X.; C. Y.; Jia, F. X.; Wu, G. F.; Hao, G. F., Cloud 3D-QSAR: a web tool for the development of quantitative structure-activity relationship models in drug discovery. *Brief. Bioinform.* **2020**, *22*, 276, DOI: 10.1093/bib/bbaa276.
- [37] Schöning-Stierand, K.; Diedrich, K.; Fährrolfes, R.; Flachsenberg, F.; Meyder, A.; Nittinger, E.; Steinegger, R.; Rarey, M., Proteins Plus: Interactive Analysis of Protein-Ligand Binding Interfaces. *Nucleic Acids Res.* **2020**, *48*, W48-W53, DOI: 10.1093/nar/gkaa235.